Mechanical Acceleration and Control of the Thermal Motion of a Magnetic Skyrmion

Yu Wang,[1,*] Takayuki Kitamura,[1] Jie Wang,[2,3] Hiroyuki Hirakata,[1] and Takahiro Shimada[1]

[1] *Department of Mechanical Engineering and Science, Kyoto University, Nishikyo-ku, Kyoto 615-8540, Japan*
[2] *Department of Engineering Mechanics, Zhejiang University, Hangzhou 310027, China*
[3] *Zhejiang Laboratory, Hangzhou 311100, China*

(Received 5 January 2022; revised 11 May 2022; accepted 20 May 2022; published 20 July 2022)

Engineering the kinetic motion of magnetic skyrmions shows great potential in spintronics. Particularly, as a natural property, temperature plays a significant role in the dynamics of skyrmions. For instance, the nonlinear and the rectilinear motions of skyrmions driven by spin-transfer torque and local energy imbalance in temperature gradients, respectively, have been explored. Although existing studies have already implied the multiphysics field-controlled property of skyrmion thermal motion, the investigation of mechanically controlled skyrmion motions in temperature gradients is absent, and the kinematic equation is unclear. Here, we employ a phase-field model to simulate the effect of mechanical strain on skyrmion motion in a temperature gradient, and demonstrate that the strain-induced anisotropic deformation of skyrmions increases the driving force and accelerates their motion. To model the mechanical effect, we propose a kinematic equation for describing the relationship between skyrmion velocity and multiphysics field variables. Lastly, the potential application of the mechanically controlled skyrmion thermal motion is demonstrated via tip indentation simulations. This work provides the thermodynamic mechanism and kinematic equation for mechanically accelerated skyrmion thermal motions, which is expected to be a guidance for future research on skyrmion dynamics and application of functional devices.

DOI: 10.1103/PhysRevApplied.18.014049

I. INTRODUCTION

A skyrmion is well known as a nanoscale local helical spin structure with topological stability, which is mainly derived from the Dzyaloshinskii-Moriya interaction (DMI) [1–4]. Due to their nanoscale nature [4], topological protection [5,6], thermodynamics stability [3], and transport [7,8], skyrmions have great potential for the future application of spintronics, like data memory [9], high-frequency signal generator [10], logical gate [11], or microwave diode [12]. Most of them are based on the transport feature of skyrmions. Therefore, for skyrmion movement, several physical tools are introduced for providing the driving force, such as electric current [13–20], mechanical loads [21–24], temperature [25–34], electric fields [35], and magnetic fields [36–43]. Particularly, as a natural property, temperature plays a significant role in skyrmion dynamics. In the literature, Kong and Zang [32] and Lin *et al.* [31] demonstrated that temperature-gradient-induced magnon current makes skyrmions move from cold to hot regions by a spin-transfer torque. Zazvorka *et al.* [28] observed a random thermal motion of skyrmions in fluctuating temperature fields. Wang *et al.* [44] demonstrated the rectilinear movement of an individual skyrmion in a temperature gradient, and found the velocity of the moving skyrmion is related to its shape. Specifically, an elliptical skyrmion, which is elongated in the temperature gradient direction, has higher velocity in the temperature gradient than a circular one. Gungordu *et al.* [45] also demonstrated that a skyrmion with deformation has variable velocity under temperature-induced magnon. Therefore, based on this, controlling the shape of a skyrmion is a promising way to control its thermal motion. As for the skyrmion shape, mechanical load, like strain, has been widely reported to have a great influence on skyrmion deformation. For instance, due to the magnetostrictive effect [46], Shibata *et al.* [47] observed the large anisotropic deformation of skyrmions in strained crystals, and Shi *et al.* [48] simulated different shapes of skyrmions in different uniaxial strain loads. Therefore, strain is regarded as a feasible way to control skyrmion thermal motion by manipulating the skyrmion shape.

Although the shape effect of skyrmion thermal motion and strain-induced skyrmion deformations have been explored separately, the study of mechanical control of thermal motion of an individual skyrmion is absent,

*wang.yu.51p@st.kyoto-u.ac.jp

and the kinematic equation including the strain effect in skyrmion thermal motion is unclear.

In this study, we employ a temperature- and mechanical-related phase-field simulation based on the Ginzburg-Landau theory to predict the acceleration of skyrmion motion in temperature gradients by uniaxial tensile strain. We find that the strain-induced anisotropic deformation of a skyrmion intensifies the local imbalance of free-energy distributions, which increases the driving force of the moving skyrmion. Based on that, we propose a kinematic equation to describe the relationship between skyrmion velocity and field variables, such as local temperature, temperature gradient, and strain. Finally, we introduce the local strain load that can control the trajectory of the moving skyrmion as one of the potential applications. Therefore, this study provides a thermodynamic discussion for mechanically controlled skyrmion motion in a temperature gradient, and derives a kinematic equation for it, which provides practical guidance for skyrmion dynamics and further motivates future works on spintronics applications.

II. PHASE-FIELD SIMULATION MODELING

In order to study the mechanical (strain) effect on skyrmion thermal motion from the viewpoint of thermodynamics, temperature- and mechanical-related real-space phase-field simulation [44,49] is employed to simulate the evolution of magnetization in ferromagnetics. In general, the dynamics of magnetization $\mathbf{M}$ is described by the Landau–Lifshitz–Gilbert (LLG) equation as

$$\frac{\partial \mathbf{M}}{\partial t} = -\gamma \mathbf{M} \times \mathbf{H}_{\text{eff}} + \frac{\alpha}{M_s} \mathbf{M} \times \frac{\partial \mathbf{M}}{\partial t}, \tag{1}$$

where $\mathbf{H}_{\text{eff}} = (-1/\mu_0)(\delta F/\delta \mathbf{M})$ is the effective magnetic field, α is the Gilbert damping, γ is the gyromagnetic ratio, M_s is the saturated magnetization, and $F = \int f dV$ is the total free energy, in which f is the free-energy density.

The total free-energy density in the ferromagnetic system is

$$\begin{aligned} f &= a(T - T_c)\mathbf{M}^2 + b\mathbf{M}^4 + A(\nabla \mathbf{M})^2 + D\mathbf{M} \cdot (\nabla \times \mathbf{M}) \\ &\quad - \frac{\mu_0}{2}\mathbf{H}^2 - \mu_0 \mathbf{H} \cdot \mathbf{M} + f_{\text{elastic}}(\boldsymbol{\varepsilon}, \mathbf{M}), \end{aligned} \tag{2.1}$$

where a and b are the Landau energy coefficients, T is temperature, T_c is the Curie temperature, A is the exchange energy coefficient, D is the DMI constant, and μ_0 is the vacuum permeability. Here $f_{\text{elastic}}(\boldsymbol{\varepsilon}, \mathbf{M})$ is the elastic energy density, which includes pure elastic and magnetostrictive energy densities as

$$\begin{aligned} f_{\text{elastic}}(\boldsymbol{\varepsilon}, \mathbf{M}) &= \frac{1}{2}C_{11}(\varepsilon_{11}^2 + \varepsilon_{22}^2 + \varepsilon_{33}^2) + C_{12}(\varepsilon_{11}\varepsilon_{22} \\ &\quad + \varepsilon_{11}\varepsilon_{33} + \varepsilon_{33}\varepsilon_{22}) + 2C_{44}(\varepsilon_{12}^2 + \varepsilon_{13}^2 + \varepsilon_{23}^2) \\ &\quad - \frac{3\lambda_{100}}{2M_s^2}(C_{11} - C_{12})(\varepsilon_{11}M_1^2 + \varepsilon_{22}M_2^2 \\ &\quad + \varepsilon_{33}M_3^2) - \frac{6\lambda_{111}}{M_s^2}C_{44}(\varepsilon_{12}M_1M_2 \\ &\quad + \varepsilon_{23}M_3M_2 + \varepsilon_{13}M_1M_3),) \end{aligned} \tag{2.2}$$

where C_{11}, C_{12}, and C_{44} are the elastic constants and λ_{100} and λ_{111} are the magnetostrictive coefficients. This is a classical magnetoelastic coupling term, which successfully describes the strain-related deformation, phase transition, and switching of skyrmions [48,50]. The detail of all free-energy densities is presented in the Supplemental Material [51].

By the overdamped assumption [52–56], the governing Eq. (1) can be reduced to the form

$$\frac{1}{L}\frac{\partial \mathbf{M}}{\partial t} = -\frac{\delta F}{\delta \mathbf{M}}, \tag{3}$$

where $L = \gamma M_s/\alpha\mu_0$ is the kinetic coefficient and $(\delta F/\delta M_i) = (\partial f/\partial M_i) - (\partial/\partial x_j)(\partial f/\partial M_{i,j})$, in which $i, j = 1, 2, 3$, representing x, y, and z directions, respectively. Both experimental observation [34] and previous simulation [44] demonstrated that the overdamped assumption is applicable for describing skyrmion thermal motion in temperature gradients. In addition to the LLG equation, the mechanical equilibrium equation

$$\frac{\partial \sigma_{ij}}{\partial x_j} = \frac{\partial}{\partial x_j}\left(\frac{\partial f}{\partial \varepsilon_{ij}}\right) = 0 \tag{4}$$

and Maxwell's equation

$$\frac{\partial B_i}{\partial x_i} = \frac{\partial}{\partial x_i}\left(-\frac{\partial f}{\partial H_i}\right) = 0 \tag{5}$$

need to be satisfied for the stresses σ_{ij} and magnetic induction B_i in ferromagnetic materials. A nonlinear finite element method is used to solve governing Eqs. (3)–(5). The detail of the finite element method is presented in the Supplemental Material [51]. Based on this phase-field model, static skyrmion phase diagrams [49] and dynamic skyrmion thermal diffusion [44] were successfully simulated in previous studies, and all of these results are consistent with experimental observations [34,57], which verifies the reliability of this temperature- and mechanical-related phase-field model.

III. RESULTS AND DISCUSSION

A. Acceleration of rectilinear skyrmion thermal motion by uniaxial strain

At first, to study the strain-controlled skyrmion motion in a temperature gradient, the trajectories of moving skyrmions are shown in Fig. 1(a), which shows motion snapshots at different time steps of 0.7, 2.8, and 5.6 ns. The specimen model of this work is a MnSi nanobar (material parameters [44,58–60] of simulations are given in the Supplemental Material [51]) with dimensions of 210, 100, and 5 nm in length, width, and thickness directions, respectively. Cartesian coordinates are introduced for showing the position in the specimen model. In detail, the upper and lower edges are at $y = 50$ and -50 nm, and the left and right edges are at $x = -100$ and 110 nm, respectively. The width direction, i.e., y direction, of the specimen has the periodic boundary condition, while other boundaries are free boundaries. When a perpendicular magnetic field ($H_z = -3.0 \times 10^5$ A/m) is applied, a stable skyrmion exists at the left side of the specimen, which is the initial state of the following simulations. Based on that, we apply an inhomogeneous temperature field to the specimen, in which the local temperature at the left edge is 20 K, and the temperature linearly decreases from the left to right edge along the length direction, i.e., x direction, with a constant temperature gradient $\nabla T = 0.04$ K/nm. In Fig. 1(a), under this temperature gradient (and uniaxial strain $\varepsilon_x = 0.5\%$), the initial stationary skyrmion moves from the left hot side to the right cold side. By comparing the results of specimens with and without strain, the skyrmion with tensile strain in the direction of the temperature gradient has higher velocity, and still has a straight trajectory. Although it has been demonstrated that homogeneous strain cannot be the driving force of skyrmion motions, the result here indicates that it can accelerate the skyrmion thermal motion in temperature gradients. To further study the strain-induced acceleration of moving skyrmions in temperature gradients, different tensile strains from 0.3% to 0.5% are applied to the specimen with temperature gradient $\nabla T = 0.04$ K/nm. Under different strain loads, the skyrmion retains a straight trajectory from the hot to cold side. In Fig. 1(b), the positions of the moving skyrmion in the x coordinate for different time steps and strain loads are shown in detail. The result shows that the skyrmion velocity increases with an increase of uniaxial strain along the temperature gradient direction, which implies that a homogeneous mechanical load can control the speed of the skyrmion thermal motion. Such accelerated directional skyrmion motion is a great advantage for the implementation of skyrmion-based memory because of its controllable velocity and straight trajectory.

B. Mechanism of strain acceleration of skyrmion thermal motion

We discuss the mechanism of strain acceleration of skyrmion thermal motion in this section. In a previous study, Wang *et al.* [44] demonstrated that the local energy imbalance of the skyrmion is the driving force of skyrmion thermal motion. Specifically, the temperature gradient and the skyrmion shape can induce an asymmetry of local free energy of the skyrmion, which can excite the motion of it. Here, to compare the driving force of the moving skyrmions of this work, the contour maps of Figs. 2(a) and 2(b) show the local free energy of the skyrmion in a temperature gradient (0.04 K/nm) without and with 0.5% uniaxial strain, respectively. They show that the magnitude of total energy density of the skyrmion with strain is higher than that without strain due to the external load. However, the applied homogeneous strain increases the free energy uniformly, hence does not contribute to the energy imbalance of both sides of the skyrmion. According to the report of Wang *et al.* [44], the energy imbalance mainly comes from the inhomogeneous temperature field and skyrmion shape. In Fig. 2, the skyrmions with and without strain are

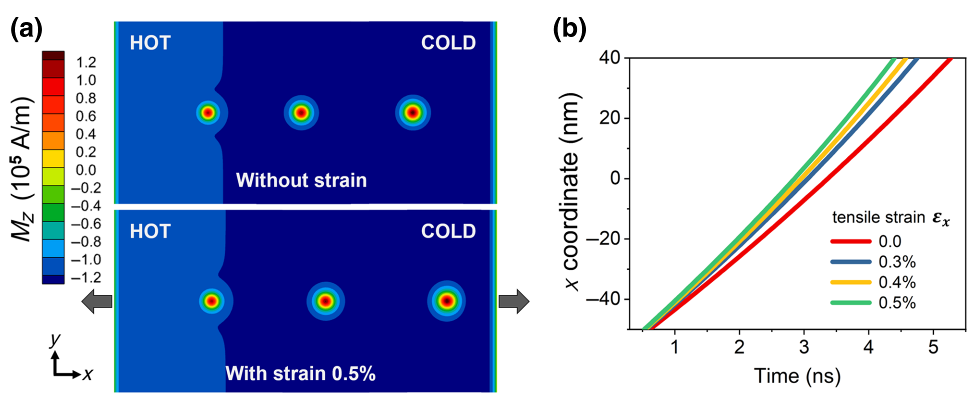

FIG. 1. (a) The diffusions of an individual skyrmion from left to right side in a constant temperature gradient (0.04 K/nm) without and with a uniaxial strain $\varepsilon_x = 0.5\%$. (b) The position of the moving skyrmion in the x coordinate for different time steps and strain loads.

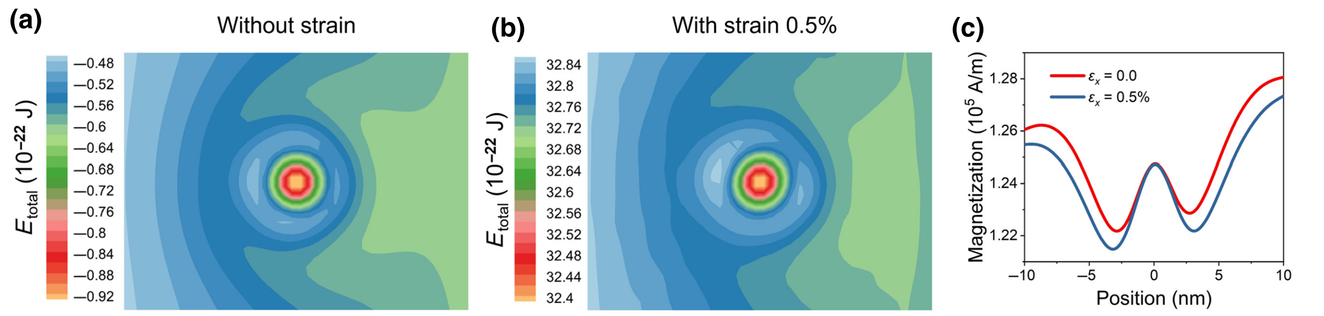

FIG. 2. Contour maps of the local free energy of a skyrmion in a temperature gradient (0.04 K/nm) without strain load (a) and with 0.5% uniaxial strain (b). (c) The magnetization distribution of skyrmions with or without strain in a temperature gradient (0.04 K/nm).

in the same temperature field (local temperature is 16 K and temperature gradient is 0.04 K/nm), so the main difference of energy imbalance between them comes from their shape. To show their shapes, Fig. 2(c) displays the magnetization distribution of the skyrmions of Figs. 2(a) and 2(b), and the result confirms that the skyrmion structure is elongated by the tensile strain. The strain-elongated elliptical skyrmion occupies more area along the temperature gradient direction, and therefore has a higher asymmetry of free energy of both sides of the skyrmion, leading to a higher driving force.

This section thus demonstrates that the strain-induced skyrmion deformation increases the asymmetry of the local free energy, which increases the driving force of the skyrmion thermal motion and thus accelerates the skyrmion.

C. Kinematic equation of moving skyrmions in temperature gradients with uniaxial strain load

Next, a kinematic equation is proposed for describing the mechanically influenced thermal motion of skyrmions. In the literature, a kinematic equation is proposed for asymmetric skyrmion motion under temperature-induced magnon [45,61]. In this work, the driving force of skyrmion thermal motion is from the imbalance of energy and the structure of the skyrmions. In a previous study

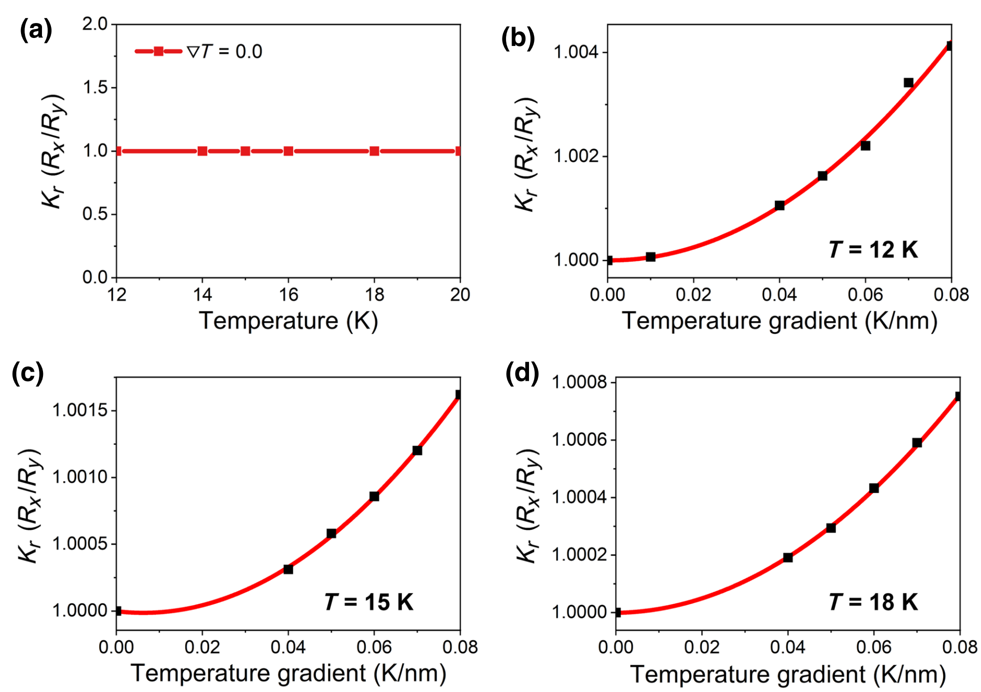

FIG. 3. (a) The relationship between skyrmion shape K_r and local temperature T when applied strain and temperature gradient are both zero. The relationship between skyrmion shape K_r and temperature gradient T when local temperature is 12 K (b), when local temperature is 15 K (c), and when local temperature is 18 K (d). The black squares are data points, and the red lines are quadratic fitting curves.

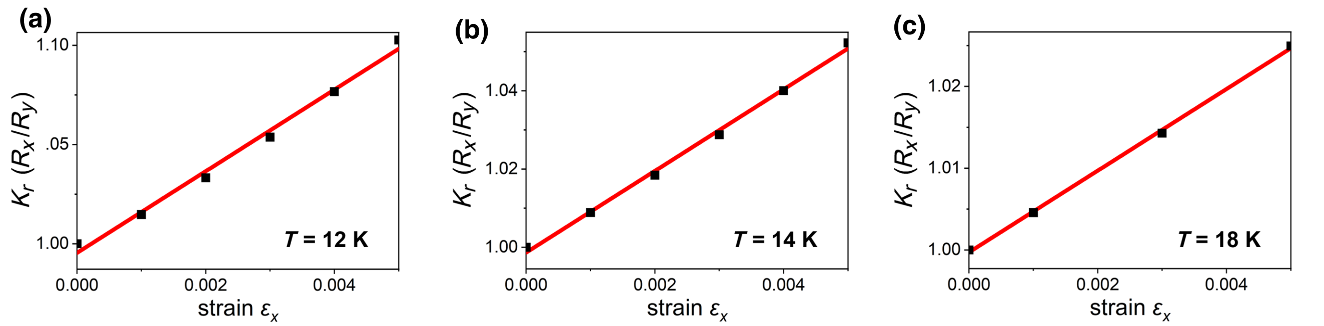

FIG. 4. The relationship between skyrmion shape K_r and uniaxial strain ε when there is no temperature gradient for 12 K (a), 14 K (b), and 18 K (c). The black squares are data points, and the red lines are linear fitting lines.

[44], a kinematic equation was proposed for the imbalanced structure-induced skyrmion thermal motion, which is dependent on the temperature gradient, local temperature, and skyrmion shape as

$$v_{\rm sk} = f\,(K_r)\nabla T(c_1 T + c_2), \tag{6}$$

where $v_{\rm sk}$ is the velocity of skyrmion thermal motion, ∇T is the temperature gradient, T is the local temperature, c_1 and c_2 are material coefficients, and $K_r = R_x/R_y$, in which R_x and R_y are the skyrmion diameters in x and y directions. Therefore, K_r can describe the skyrmion shape ($K_r = 1$ when the skyrmion is circular). The specific form of $f\,(K_r) = c_3K_r + c_4$ can amend the skyrmion shape effect on skyrmion thermal motion, where c_3 and c_4 are material coefficients. Therefore, Eq. (6) can be written as

$$v_{\rm sk} = (c_3K_r + c_4)\nabla T(c_1T + c_2). \tag{7}$$

Based on the previous conclusion, we demonstrate that the skyrmion shape K_r is determined by field variables like temperature gradient ∇T, local temperature T, and strain ε, and the mechanical effect on skyrmion thermal motion is only included via the strain-controlled skyrmion shape. Therefore, to complete the kinematic Eq. (7), the specific form of skyrmion shape $K_r(T, \nabla T, \varepsilon)$ is investigated next. At first, we only consider the effect of temperature. As shown in Fig. 3(a), when strain $\varepsilon = 0$ and temperature gradient $\nabla T = 0$, K_r is always equal to 1.0 at different temperatures, which means the skyrmion shape remains circular if there is no temperature gradient and applied strain. Figures 3(b)–3(d) show the relationship between skyrmion shape K_r and temperature gradient for different local temperatures without applied strain. According to the results, K_r and temperature gradient exhibit a quadratic relationship no matter the local temperature.

Based on these features, the skyrmion shape without applied strain $K_r(T, \nabla T, \varepsilon = 0)$ can be described by field variables as

$$K_r(T, \nabla T, \varepsilon = 0) = \alpha(T) \cdot \nabla T^2 + 1, \tag{8}$$

where $\alpha(T)$ is a function of temperature T. According to Eq. (8), when temperature gradient $\nabla T = 0$, K_r equals 1.0, and when local temperature is a constant, K_r and temperature gradient show a quadratic relationship, which is consistent with the features revealed in Fig. 3. Then, based on phase-field simulations, the specific form of $\alpha(T)$ can be

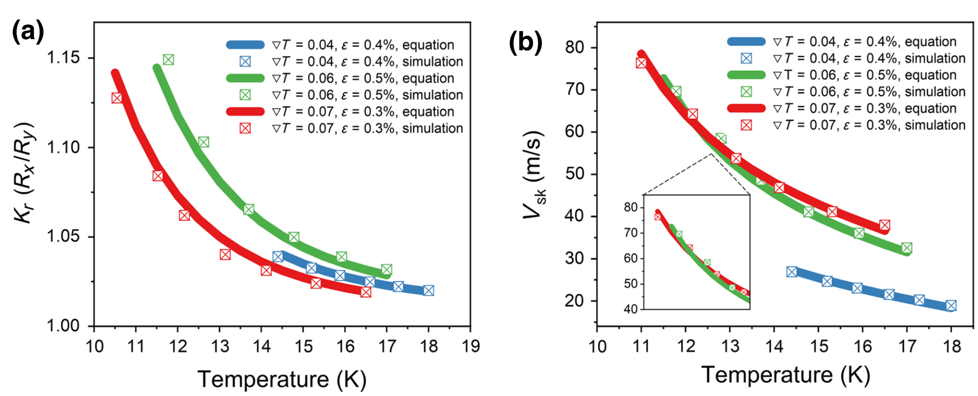

FIG. 5. (a) The results of skyrmion shape K_r obtained from both Eq. (11) and phase-field simulations. (b) The results of skyrmion velocity $v_{\rm sk}$ obtained from both kinematic Eq. (12) and phase-field simulations. The enlarged inset shows the detail of the overlapped area. In both panels, solid lines and crossed squares represent the results from equation and phase-field simulation, respectively.

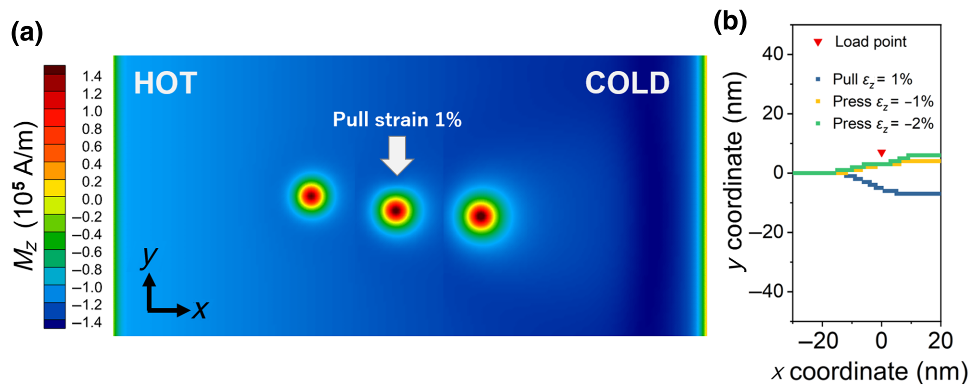

FIG. 6. (a) The trajectory of a moving skyrmion is changed by a local out-of-plane pull strain load. (b) The trajectory of a moving skyrmion in different local out-of-plane strain loads. The red triangle shows the loading point (0, 6).

expressed by an empirical function: $\alpha(T) = c_5 T^{c_6}$, where c_5 and c_6 are material coefficients. Therefore, Eq. (8) can be written as

$$K_r(T, \nabla T, \varepsilon = 0) = c_5 T^{c_6} \cdot \nabla T^2 + 1. \tag{9}$$

Then, we include the uniaxial strain effect on the skyrmion shape $K_r(T, \nabla T, \varepsilon)$. Considering the temperature gradient and the strain have an independent effect on skyrmion shape, the strain effect on skyrmion shape can thus be expressed with an additional term as

$$K_r(T, \nabla T, \varepsilon) = c_5 T^{c_6} \cdot \nabla T^2 + 1 + g(\varepsilon), \tag{10}$$

where ε is uniaxial strain ($\varepsilon > 0$) and $g(\varepsilon)$ is a function for the effect of strain on skyrmion shape. To find the specific form of $g(\varepsilon)$, the relationship between skyrmion shape K_r and uniaxial strain ε is shown in Fig. 4. To only consider the strain effect, the temperature gradient is set as 0 here. Then, the result shows that K_r increases with strain linearly for different constant temperatures (and when strain equals 0, K_r always equals 1). Therefore, $g(\varepsilon)$ can be expressed in the form of $g(\varepsilon) = \beta(T) \cdot \varepsilon$. Similarly, $\beta(T)$ can be expressed as a power function: $\beta(T) = c_7 T^{c_8} + c_9$, where c_7, c_8, and c_9 are material coefficients. Therefore, Eq. (10) can be written as

$$K_r(T, \nabla T, \varepsilon) = c_5 T^{c_6} \cdot \nabla T^2 + (c_7 T^{c_8} + c_9) \cdot \varepsilon + 1, \tag{11}$$

which shows the specific relationship between skyrmion shape and physical fields.

To check the accuracy of Eq. (11), Fig. 5(a) shows the results of the skyrmion shape K_r that come from both Eq. (11) and phase-field simulation. As expected, the result of Eq. (11) is well consistent with the simulation. The largest error is only around 1.5%. Substituting the K_r term of Eq. (7) by Eq. (11), the kinematic equation of the mechanically controlled skyrmion thermal motion is written as

$$v_{sk}(T, \nabla T, \varepsilon) = \nabla T(c_1 T + c_2)[c_3(c_5 T^{c_6} \cdot \nabla T^2 + (c_7 T^{c_8} + c_9) \cdot \varepsilon + 1) + c_4], \tag{12}$$

where c_1 to c_9 are material coefficients. They are obtained from nine data points of phase-field simulations (the details of c_1 to c_9 are given in the Appendix). To check the accuracy, Fig. 5(b) shows the results of the skyrmion velocity v_{sk}, obtained from both kinematic Eq. (12) and phase-field simulations. In this figure, the result of Eq. (12) is well consistent with the simulation at different temperature gradients, local temperatures, and strain loads. Therefore, we have successfully built a kinematic equation that describes mechanically controlled skyrmion thermal motion in terms of field variables (like local temperature, temperature gradient, and uniaxial strain). Although the one-dimensional equation cannot cover all possible situations, it reveals the thermodynamic mechanism of mechanically controlled skyrmion thermal motion from an energy analysis, which is a start point for the further construction of systematic and sophisticated kinematic equations. Therefore, it is a theoretical guidance for future research of skyrmion dynamics.

D. Potential application of mechanically controlled skyrmion thermal motion

According to the kinematic Eq. (12), the strain load can control the dynamic behavior of skyrmions in a temperature gradient. Although only homogeneous strain is discussed in the previous sections, an inhomogeneous strain field is expected to generate more complex energy imbalance, then leading to the novel dynamic behavior of moving skyrmions. As shown in Fig. 6(a), a local out-of-plane pull strain of 1% is applied at the position (0, 6), which generates a relatively complex strain (gradient) field at this local area. When skyrmion moves near this area, the complex strain field can even change its trajectory. Figure 6(b) shows the trajectory of the moving skyrmion for different local strain loads. The result shows the moving skyrmion can be attracted by local out-of-plane press strain and be repelled by pull strain, which indicates that the strain gradient field has a more complex effect on skyrmion dynamics, and mechanically controlled skyrmion thermal motion has enormous potential in the application of spintronic devices such as racetrack memory, due to controllable velocity and trajectory.

IV. CONCLUSION

In conclusion, we show the acceleration of rectilinear skyrmion thermal motion in temperature gradients by uniaxial strain. The strain-induced skyrmion deformation increases the energy asymmetry of the skyrmion, which intensifies the driving force of skyrmion thermal motion. Further, we propose a kinematic equation for describing mechanically controlled skyrmion motion under temperature gradients by field variables. Finally, the potential application of memory devices is proposed. This study shows a simulation method for temperature- and mechanical-related skyrmion behaviors, and proposes a thermodynamic discussion and kinematic equation about mechanically controlled skyrmion thermal motion. Our results may inspire future study of field-controlled skyrmion thermal motion and moving skyrmions in multiphysics fields (like electromagnetic fields, strain gradients, and waves). Therefore, we expect this study to be a theoretical support for skyrmion dynamics and skyrmion-based spintronics.

ACKNOWLEDGMENTS

The authors acknowledge financial support from JSPS KAKENHI (Grants No. 18H05241, No. 20H05653, No. 20H02027, No. 20H05190, and No. 21K18673). J.W. acknowledges financial support from Key Research Project of Zhejiang Laboratory (Grant No. 2021PE0AC02).

APPENDIX

The values of material coefficients c_1 to c_9 of empirical kinematic Eq. (12) for a MnSi nanobar are as follows: $c_1 = -0.138125$, $c_2 = 3.940625$ K, $c_3 = 1.603768212 \times 10^{-6}\ \mathrm{K}^{-2}\,\mathrm{m}^2\,\mathrm{s}^{-1}$, $c_4 = -1.318207861 \times 10^{-6}\ \mathrm{K}^{-2}\,\mathrm{m}^2\,\mathrm{s}^{-1}$, $c_5 = 5.50817 \times 10^{-13}\ \mathrm{K}^{3.3675}\,\mathrm{m}^2$, $c_6 = -5.3675$, $c_7 = 1.31341 \times 10^7\ \mathrm{K}^{5.38372}$, $c_8 = -5.38372$, and $c_9 = 2.52849$.

[1] I. Dzyaloshinsky, A thermodynamic theory of “weak” ferromagnetism of antiferromagnetics, J. Phys. Chem. Solids **4**, 241 (1958).

[2] T. Moriya, Anisotropic superexchange interaction and weak ferromagnetism, Phys. Rev. **120**, 91 (1960).

[3] U. K. Rößler, A. N. Bogdanov, and C. Pfleiderer, Spontaneous skyrmion ground states in magnetic metals, Nature **442**, 797 (2006).

[4] X. Z. Yu, Y. Onose, N. Kanazawa, J. H. Park, J. H. Han, Y. Matsui, N. Nagaosa, and Y. Tokura, Real-space observation of a two-dimensional skyrmion crystal, Nature **465**, 901 (2010).

[5] S. Heinze, K. Von Bergmann, M. Menzel, J. Brede, A. Kubetzka, R. Wiesendanger, G. Bihlmayer, and S. Blügel, Spontaneous atomic-scale magnetic skyrmion lattice in two dimensions, Nat. Phys. **7**, 713 (2011).

[6] A. Fert, N. Reyren, and V. Cros, Magnetic skyrmions: Advances in physics and potential applications, Nat. Rev. Mater. **2**, 17031 (2017).

[7] S. Zhang and Z. Li, Roles of Nonequilibrium Conduction Electrons on the Magnetization Dynamics of Ferromagnets, Phys. Rev. Lett. **93**, 1 (2004).

[8] W. Jiang, P. Upadhyaya, W. Zhang, G. Yu, M. B. Jungfleisch, F. Y. Fradin, J. E. Pearson, Y. Tserkovnyak, K. L. Wang, O. Heinonen, S. G. E. Te Velthuis, and A. Hoffmann, Blowing magnetic skyrmion bubbles, Science **349**, 283 (2015).

[9] S. Woo, K. Litzius, B. Krüger, M. Y. Im, L. Caretta, K. Richter, M. Mann, A. Krone, R. M. Reeve, M. Weigand, P. Agrawal, I. Lemesh, M. A. Mawass, P. Fischer, M. Kläui, and G. S. D. Beach, Observation of room-temperature magnetic skyrmions and their current-driven dynamics in ultrathin metallic ferromagnets, Nat. Mater. **15**, 501 (2016).

[10] S. Luo, Y. Zhang, M. Shen, J. Ou-Yang, B. Yan, X. Yang, S. Chen, B. Zhu, and L. You, Skyrmion-based high-frequency signal generator, Appl. Phys. Lett. **110**, 112402 (2017).

[11] S. Krause and R. Wiesendanger, Spintronics: Skyrmionics gets hot, Nat. Mater. **15**, 493 (2016).

[12] M. Mochizuki and S. Seki, Magnetoelectric resonances and predicted microwave diode effect of the skyrmion crystal in a multiferroic chiral-lattice magnet, Phys. Rev. B: Condens. Matter Mater. Phys. **87**, 1 (2013).

[13] Y. qing Zheng and Y. Wang, Continuous nucleation dynamics of magnetic skyrmions in T-shaped chiral ferromagnetic nanojunction, J. Magn. Magn. Mater. **489**, 165372 (2019).

[14] Y. Feng, J. Xia, L. Qiu, X. Cai, L. Shen, F. J. Morvan, X. Zhang, Y. Zhou, and G. Zhao, A skyrmion-based spin-torque nano-oscillator with enhanced edge, J. Magn. Magn. Mater. **491**, 165610 (2019).

[15] J. Iwasaki, M. Mochizuki, and N. Nagaosa, Universal current-velocity relation of skyrmion motion in chiral magnets, Nat. Commun. **4**, 1463 (2013).

[16] X. Z. Yu, N. Kanazawa, W. Z. Zhang, T. Nagai, T. Hara, K. Kimoto, Y. Matsui, Y. Onose, and Y. Tokura, Skyrmion flow near room temperature in an ultralow current density, Nat. Commun. **3**, 988 (2012).

[17] A. Hrabec, J. Sampaio, M. Belmeguenai, I. Gross, R. Weil, S. M. Chérif, A. Stashkevich, V. Jacques, A. Thiaville, and S. Rohart, Current-induced skyrmion generation and dynamics in symmetric bilayers, Nat. Commun. **8**, 1 (2017).

[18] S. Woo, K. M. Song, X. Zhang, Y. Zhou, M. Ezawa, X. Liu, S. Finizio, J. Raabe, N. J. Lee, S. Il Kim, S. Y. Park, Y. Kim, J. Y. Kim, D. Lee, O. Lee, J. W. Choi, B. C. Min, H. C. Koo, and J. Chang, Current-driven dynamics and inhibition of the skyrmion Hall effect of ferrimagnetic skyrmions in GdFeCo films, Nat. Commun. **9**, 9 (2018).

[19] R. Murooka, A. O. Leonov, K. Inoue, and J. ichiro Ohe, Current-induced shuttlecock-like movement of non-axisymmetric chiral skyrmions, Sci. Rep. **10**, 1 (2020).

[20] N. Nagaosa and Y. Tokura, Topological properties and dynamics of magnetic skyrmions, Nat. Nanotechnol. **8**, 899 (2013).

[21] R. Yanes, F. Garcia-Sanchez, R. F. Luis, E. Martinez, V. Raposo, L. Torres, and L. Lopez-Diaz, Skyrmion motion induced by voltage-controlled in-plane strain gradients, Appl. Phys. Lett. **115**, 1 (2019).

[22] C. Hu, R. Zhao, L. Ji, W. Chen, S. Bandaru, and X. Zhang, A universal law for predicting the motion behaviors of skyrmions under spatially-varying strain field, J. Magn. Magn. Mater. **513**, 166954 (2020).

[23] R. Nepal, U. Güngördü, and A. A. Kovalev, Magnetic skyrmion bubble motion driven by surface acoustic waves, Appl. Phys. Lett. **112**, 112404 (2018).

[24] T. Yokouchi, S. Sugimoto, B. Rana, S. Seki, N. Ogawa, S. Kasai, and Y. Otani, Creation of magnetic skyrmions by surface acoustic waves, Nat. Nanotechnol. **15**, 361 (2020).

[25] W. T. Hou, J. X. Yu, M. Daly, and J. Zang, Thermally driven topology in chiral magnets, Phys. Rev. B **96**, 1 (2017).

[26] A. F. Schäffer, L. Rózsa, J. Berakdar, E. Y. Vedmedenko, and R. Wiesendanger, Stochastic dynamics and pattern formation of geometrically confined skyrmions, Commun. Phys. **2**, 1 (2019).

[27] L. Zhao, Z. Wang, X. Zhang, X. Liang, J. Xia, K. Wu, H. A. Zhou, Y. Dong, G. Yu, K. L. Wang, X. Liu, Y. Zhou, and W. Jiang, Topology-Dependent Brownian Gyromotion of a Single Skyrmion, Phys. Rev. Lett. **125**, 27206 (2020).

[28] J. Zázvorka, F. Jakobs, D. Heinze, N. Keil, S. Kromin, S. Jaiswal, K. Litzius, G. Jakob, P. Virnau, D. Pinna, K. Everschor-Sitte, L. Rózsa, A. Donges, U. Nowak, and M. Kläui, Thermal skyrmion diffusion used in a reshuffler device, Nat. Nanotechnol. **14**, 658 (2019).

[29] M. Mochizuki, X. Z. Yu, S. Seki, N. Kanazawa, W. Koshibae, J. Zang, M. Mostovoy, Y. Tokura, and N. Nagaosa, Thermally driven ratchet motion of a skyrmion microcrystal and topological magnon Hall effect, Nat. Mater. **13**, 241 (2014).

[30] X. G. Wang, L. Chotorlishvili, V. K. Dugaev, A. Ernst, I. V. Maznichenko, N. Arnold, C. Jia, J. Berakdar, I. Mertig, and J. Barnaś, The optical tweezer of skyrmions, npj Comput. Mater. **6**, 1 (2020).

[31] S. Z. Lin, C. D. Batista, C. Reichhardt, and A. Saxena, Ac Current Generation in Chiral Magnetic Insulators and Skyrmion Motion Induced by the Spin Seebeck Effect, Phys. Rev. Lett. **112**, 1 (2014).

[32] L. Kong and J. Zang, Dynamics of an Insulating Skyrmion under a Temperature Gradient, Phys. Rev. Lett. **111**, 1 (2013).

[33] A. A. Kovalev and Y. Tserkovnyak, Thermoelectric spin transfer in textured magnets, Phys. Rev. B: Condens. Matter Mater. Phys. **80**, 1 (2009).

[34] Z. Wang, *et al.*, Thermal generation, manipulation and thermoelectric detection of skyrmions, Nat. Electron. **3**, 672 (2020).

[35] C. Ma, X. Zhang, J. Xia, M. Ezawa, W. Jiang, T. Ono, S. N. Piramanayagam, A. Morisako, Y. Zhou, and X. Liu, Electric field-induced creation and directional motion of domain walls and skyrmion bubbles, Nano Lett. **19**, 353 (2019).

[36] L. Kong, L. Bo, R. Zhao, C. Hu, L. Ji, Y. Zhang, and X. Zhang, Linear dependence of skyrmion velocity on response resonance frequency of local magnetization, Appl. Phys. Lett. **116**, 192407 (2020).

[37] J. Ding, X. Yang, and T. Zhu, The motion of magnetic skyrmions driven by propagating spin waves, IEEE Trans. Magn. **51**, 4 (2015).

[38] J. J. Liang, J. H. Yu, J. Chen, M. H. Qin, M. Zeng, X. B. Lu, X. S. Gao, and J. M. Liu, Magnetic field gradient driven dynamics of isolated skyrmions and antiskyrmions in frustrated magnets, ArXiv, f (2017).

[39] W. Wang, M. Beg, B. Zhang, W. Kuch, and H. Fangohr, Driving magnetic skyrmions with microwave fields, Phys. Rev. B: Condens. Matter Mater. Phys. **92**, 1 (2015).

[40] Y. Liu, H. Yan, M. Jia, H. Du, A. Du, and J. Zang, Field-driven oscillation and rotation of a multiskyrmion cluster in a nanodisk, Phys. Rev. B **95**, 1 (2017).

[41] M. Ikka, A. Takeuchi, and M. Mochizuki, Resonance modes and microwave-driven translational motion of a skyrmion crystal under an inclined magnetic field, Phys. Rev. B **98**, 1 (2018).

[42] C. Psaroudaki and D. Loss, Skyrmions Driven by Intrinsic Magnons, Phys. Rev. Lett. **120**, 237203 (2018).

[43] S. Fin, R. Silvani, S. Tacchi, M. Marangolo, L. C. Garnier, M. Eddrief, C. Hepburn, F. Fortuna, A. Rettori, M. G. Pini, and D. Bisero, Straight motion of half-integer topological defects in thin Fe-N magnetic films with stripe domains, Sci. Rep. **8**, 1 (2018).

[44] Y. Wang, T. Shimada, J. Wang, T. Kitamura, and H. Hirakata, The rectilinear motion of the individual asymmetrical skyrmion driven by temperature gradients, Acta Mater. **221**, 117383 (2021).

[45] U. Güngördü, R. Nepal, O. A. Tretiakov, K. Belashchenko, and A. A. Kovalev, Stability of skyrmion lattices and symmetries of quasi-two-dimensional chiral magnets, Phys. Rev. B **93**, 1 (2016).

[46] J. Wang, Mechanical control of magnetic order: From phase transition to skyrmions, Annu. Rev. Mater. Res. **49**, 361 (2019).

[47] K. Shibata, J. Iwasaki, N. Kanazawa, S. Aizawa, T. Tanigaki, M. Shirai, T. Nakajima, M. Kubota, M. Kawasaki, H. S. Park, D. Shindo, N. Nagaosa, and Y. Tokura, Large anisotropic deformation of skyrmions in strained crystal, Nat. Nanotechnol. **10**, 589 (2015).

[48] J. Wang, Y. Shi, and M. Kamlah, Uniaxial strain modulation of the skyrmion phase transition in ferromagnetic thin films, Phys. Rev. B **97**, 1 (2018).

[49] Y. Wang and J. Wang, The temperature-strain phase diagrams of ferromagnetic thin films under different magnetic fields, J. Phys. Condens. Matter **33**, 235802 (2021).

[50] J.-M. Hu, T. Yang, and L.-Q. Chen, Strain-mediated voltage-controlled switching of magnetic skyrmions in nanostructures, npj Comput. Mater. **4**, 62 (2018).

[51] See Supplemental Material at http://link.aps.org/supplemental/10.1103/PhysRevApplied.18.014049 for more

information concerning free energy, the finite element method, material parameters, and the $M(T)$ curve.

[52] J. Wang and J. Zhang, A real-space phase field model for the domain evolution of ferromagnetic materials, Int. J. Solids Struct. **50**, 3597 (2013).

[53] Y. Wang, J. Sun, T. Shimada, H. Hirakata, T. Kitamura, and J. Wang, Ferroelectric control of magnetic skyrmions in multiferroic heterostructures, Phys. Rev. B **102**, 14440 (2020).

[54] A. Gordon, I. D. Vagner, and P. Wyder, Kinetics of diamagnetic phase transitions, Phys. Rev. B **41**, 658 (1990).

[55] Y. Ni, L. He, and A. G. Khachaturyan, Equivalency principle for magnetoelectroelastic multiferroics with arbitrary microstructure: The phase field approach, J. Appl. Phys. **108**, 023504 (2010).

[56] X. Lu, H. Li, and B. Wang, Theoretical analysis of electric, magnetic and magnetoelectric properties of nano-structured multiferroic composites, J. Mech. Phys. Solids **59**, 1966 (2011).

[57] S. Mühlbauer, B. Binz, F. Jonietz, C. Pfleiderer, A. Rosch, A. Neubauer, R. Georgii, and P. Böni, Skyrmion lattice in a chiral magnet, Science **323**, 915 (2009).

[58] Y. Hu and B. Wang, Unified theory of magnetoelastic effects in B20 chiral magnets, New J. Phys. **19**, 123002 (2017).

[59] J. M. Hu, T. Yang, and L. Q. Chen, Stability and dynamics of skyrmions in ultrathin magnetic nanodisks under strain, Acta Mater. **183**, 145 (2020).

[60] J. Miltat, S. Rohart, and A. Thiaville, Brownian motion of magnetic domain walls and skyrmions, and their diffusion constants, Phys. Rev. B **97**, 1 (2018).

[61] A. A. Kovalev, Skyrmionic spin Seebeck effect via dissipative thermomagnonic torques, Phys. Rev. B: Condens. Matter Mater. Phys. **89**, 1 (2014).